THE CRATERING RECORD ON MERCURY AND THE ORIGIN OF IMPACTING OBJECTS

ROBERT G. STROM
University of Arizona

and

GERHARD NEUKUM
German Aerospace Research Establishment

The heavily cratered highlands of Mercury, Mars and the Moon all have similar crater size-frequency distributions. However, the Mercurian highlands show a marked paucity of craters < 50 km diameter compared to the lunar highlands. The paucity can be explained by crater obliteration by intercrater plains emplacement on Mercury and indicates that Mercury's intercrater plains were formed during the period of late heavy bombardment. They may range in age from about 4 to 4.2 Gyr. The post-Caloris crater population is similar to that of the lunar highlands over the same diameter range but has a much lower crater density than the lunar or Mercurian highlands, and a significantly higher density than the lunar maria. Unlike the lunar maria, Mercury's smooth plains were probably emplaced near the end of late heavy bombardment. Mercury's volcanic activity was very intense early in its history (much more so than the Moon) but ended sooner on Mercury (≈ 3.8 Gyr ago) than on the Moon. This is probably the consequence of the formation of Mercury's enormous iron core which caused extensive melting, global expansion and crustal tension during the period of late heavy bombardment, followed by cooling and global contraction to shut off magma sources early in its history. A comparison of the inner solar system cratering record with that at Jupiter shows that the heavily cratered surfaces of Ganymede and Callisto have a different crater population which cannot be explained by differences in crater scaling. The impact velocities needed to match the Callisto and lunar crater curves are completely unrealistic

for objects in heliocentric orbits that cross both Jupiter and the inner planets. Furthermore, the lateral displacements of the crater curves for the terrestrial planet highlands require impact velocity differences between Mercury, the Moon, and Mars that can only be explained by objects with small semimajor axes confined to the inner solar system. These results suggest that the objects responsible for the period of late heavy bombardment on the terrestrial planets were accretional remnants left over from the formation of the terrestrial planets and confined to the inner solar system. The cratering record in the outer solar system may have been produced largely by objects in planetocentric orbits.

The cratering record on Mercury provides information on geologic processes, time scales and the origin of impacting objects. Mariner 10 images showed that, like the Moon and Mars, Mercury has a heavily cratered surface. This demonstrated that all of the inner planets, including the Earth and Venus, experienced a period of late heavy bombardment early in solar system history. Mercury's cratering record is important because it provides information on the impact history in the innermost region of the solar system.

Various aspects of the solar system cratering record, sometimes with widely disparate conclusions, have been discussed by Chapman and McKinnon (1986), Strom (1987a), Plescia and Boyce (1985), Shoemaker and Wolfe (1982), Neukum (1985), Hartmann (1984), Woronow (1978) and Horedt and Neukum (1984). These are by no means the only papers that discuss the cratering record of the solar system, but the reader is referred to these for different views on the origin of impacting objects and cratering processes. In particular, the reader is referred to the chapter in *Satellites* by Chapman and McKinnon (1986) for an excellent summary of the various viewpoints and the uncertainties in interpreting the cratering record.

This chapter is largely confined to a discussion of the terrestrial planet cratering record with emphasis on Mercury. First we review the geologic units on Mercury most relevant to the cratering record (Sec. I). In Sec. II the issue of equilibrium and saturation is reviewed and some new observations are presented. This is followed by a discussion of the Mercurian cratering record and its implications for geologic processes (Sec. III). Absolute time scales on the Moon and Mercury are considered in Sec. IV. The origin of the objects responsible for the period of late heavy bombardment in the inner solar system is discussed in Sec. V.

Two types of crater size-frequency distribution plots are used in this chapter: (1) the cumulative plot, and (2) the relative or "R" plot. In the cumulative size-distribution, the log cumulative crater frequency is plotted against the log crater diameter and is in the form $N \propto D^{\alpha}$ where N is the cumulative crater frequency, D is the crater diameter and α is the population or slope index. The "R" plot displays information on the differential size distribution, and is the ratio of the observed distribution to the function $dN \propto D^{-3}\, dD$. Because most large crater populations have slope or population indices within the range of ± 1 of the function D^{-3}, they plot as nonsloping or

moderately sloping lines on these log/log plots. On an "R" plot, a horizontal line has a differential −3 slope index; one sloping down to the left at an angle of 45° has a differential −2 slope index and one sloping down to the right at 45° has a differential −4 slope index. The vertical position of the curve is a measure of crater density: the higher the curve, the greater the crater density. For a given single-sloped cumulative slope index, the equivalent differential slope index is decreased by 1, e.g., a cumulative −2 slope index is equivalent to a differential −3 slope index, a cumulative −1 is a differential −2, etc. The most frequently used plot in this chapter is the "R" plot, and therefore we will refer only to the differential population index.

I. GEOLOGIC UNITS

Like the Moon and Mars, Mercury's surface can be broadly divided into two physiographic provinces: highlands and lowland plains. The highlands of Mercury consist of heavily cratered areas interspersed with broad areas of gently rolling plains superposed with a high density of craters less than about 15 km diameter. These highland plains have been termed intercrater plains (Trask and Guest 1975). They occupy about 45% of the surface viewed by Mariner 10, and therefore constitute the major terrain type on Mercury. Many of the superposed small craters form chains or clusters suggestive of secondary impact craters. Both the Moon and Mars also have intercrater plains. On the Moon, however, the old (pre-Imbrium) intercrater plains are much less extensive than on Mercury and Mars.

The Mercurian lowland plains occur primarily within and surrounding the Caloris basin and in the north polar region. They have been termed smooth plains by Trask and Guest (1975). Smooth plains also occur on the floors of other large basins such as Tolstoij and Beethoven and as patches in the highlands. They resemble the lunar maria in both morphology and mode of occurrence. The albedo and color of the smooth plains differ significantly from those of the lunar maria (Strom 1984; Hapke et al. 1980; Hapke et al. 1975). The Caloris smooth plains are about 90% brighter than the lunar maria and the color differences are less than those within the lunar maria. The density of craters superposed on the smooth plains is considerably less than that on the intercrater plains indicating that they are younger. Their younger age is also confirmed by stratigraphic relationships (see chapter by Spudis and Guest).

Other geologic units occur on Mercury and are discussed in detail by Spudis and Guest in their chapter on the stratigraphy and geologic history. However, the Mercurian highlands with its extensive intercrater plains unit and the smooth plains are most relevant to the cratering record on Mercury. The origins of these two plains units are somewhat controversial. Both units have been ascribed to either volcanism or to basin-forming ejecta deposits. The evidence for these two very different origins has been reviewed by Strom (1984) and also in the chapter by Spudis and Guest. Current evidence seems to

favor a volcanic origin for both plains units, but the evidence is considerably stronger for the smooth plains than for the intercrater plains. The reader is referred to the chapter by Spudis and Guest for a thorough discussion of this topic.

II. THE ISSUE OF SATURATION, STEADY STATE AND EQUILIBRIUM

There has long been a scientific debate in the field of impact cratering studies about the highest crater densities on the most ancient surfaces of the terrestrial planets and outer planet satellites. One school of thought believes these crater populations are saturated or in steady state (see, e.g., Hartmann 1984), while the other believes they are not (see, e.g., Woronow 1978). The concept of saturation is relatively simple. It merely means that a surface is so heavily cratered that each new crater destroys others in such a way that the crater density remains constant or nearly constant no matter how many craters are added. Thus, the surface is in a steady state or has reached equilibrium. Although this concept is simple, the process by which saturation occurs and the crater density or densities at which it takes place is quite complex.

The central issue for our purposes is *not* whether a surface is saturated, but *whether the observed crater size-frequency distribution is essentially the same as, or close to, the production size-frequency distribution.* A production size-frequency distribution is one that has retained its original form, and, therefore, reflects the projectile size-frequency distribution. In the absence of extensive erosion and deposition, a lightly cratered surface preserves the crater production population. Even on surfaces where craters have been destroyed by the cratering process, the production size-frequency distribution can still be preserved (Neukum and Dietzel 1971; Chapman and McKinnon 1986; Woronow 1977,1978). If one is dealing with a production population, then the projectile size-frequency distribution can be recovered by providing the correct values to parameters in an appropriate crater scaling law.

There are essentially two ways a production size-frequency distribution can be changed. One is by geologic (endogenic) processes such as erosion and deposition that destroy pre-existing craters, and the other is by the cratering process itself. Depositional and erosional processes destroy small craters more easily than large craters, resulting in a preferential loss of small craters relative to large ones. This results in an increase in the population index at smaller crater sizes, i.e., the slope index becomes less negative. At an extreme, all craters smaller than some threshold diameters may be destroyed. Another geologic process that can change the production population is the destruction of larger craters by viscous relaxation on icy surfaces. In this case, the population index decreases (becomes more negative) at larger crater diameters. Again, at the extreme, all craters larger than some threshold diameter may disappear.

The production size-frequency distribution can also change as saturation is approached and attained depending on the population index of the production population. For single-slope production size-frequency distributions with population indices more negative than -3, the population index increases (becomes less negative) as saturation is reached or approached. But this is not true for "shallower" initial size-frequency distributions. For example, production size frequencies with population indices equal to or less negative than about -2.5 retain their population indices at saturation (Woronow 1977). Neukum and Dietzel (1971) reached similar conclusions using an analytical approach.

Figures 1 and 2 show the crater size-frequency distributions for the lunar, Mercurian, and Martian highlands. They all display a complex curve of similar shape that cannot be represented by a single-slope population index. Between about 10 and 50 km diameter, the population index α is -2, at sizes between 50 and 150 km it is -3, at sizes 150 to 250 km it is about -4, and at diameters greater than about 300 km it is approximately -2, although the statistics are quite poor at these sizes.

The central question concerns the most heavily cratered surfaces in the solar system and whether or not they retain the signature of their production populations. There are two methods of addressing this problem: computer modeling and observation. The modeling approach concerns Monte Carlo computer simulations which crater a surface with size-frequency distributions of single or multiple population indices until that surface is saturated, i.e., the crater density stays nearly constant. Such simulations have been performed by Woronow (1977,1978) and by Chapman (Chapman and McKinnon 1986). The reader is referred to these publications for details and results of the simulations and thorough reviews of previous studies. The main difference between the simulation results is that Woronow found that saturation occurs at crater densities considerably higher than those observed on the most heavily cratered surfaces, while Chapman, using a somewhat different set of parameters, found that saturation occurs at lower crater densities closer to those observed. The difference between the two results appears to be due to the model parameters which govern the efficiency with which craters are destroyed. The values used by Woronow favor a lesser efficiency for destroying craters than those used by Chapman. The selection of these values is somewhat subjective. Chapman's values may be more realistic but the truth may lie somewhere between the two models. Probably all that can be said at this time is that the heavily cratered surfaces in the solar system may be relatively close to saturation density, but whether or not they have actually reached equilibrium is uncertain.

There are, however, certain results from these computer simulations that seem to be well founded. For a shallow-sloped (index > -3) production population of large dynamic range (large differences in crater sizes), the surface reaches only a state of quasi-equilibrium because crater obliteration is domi-

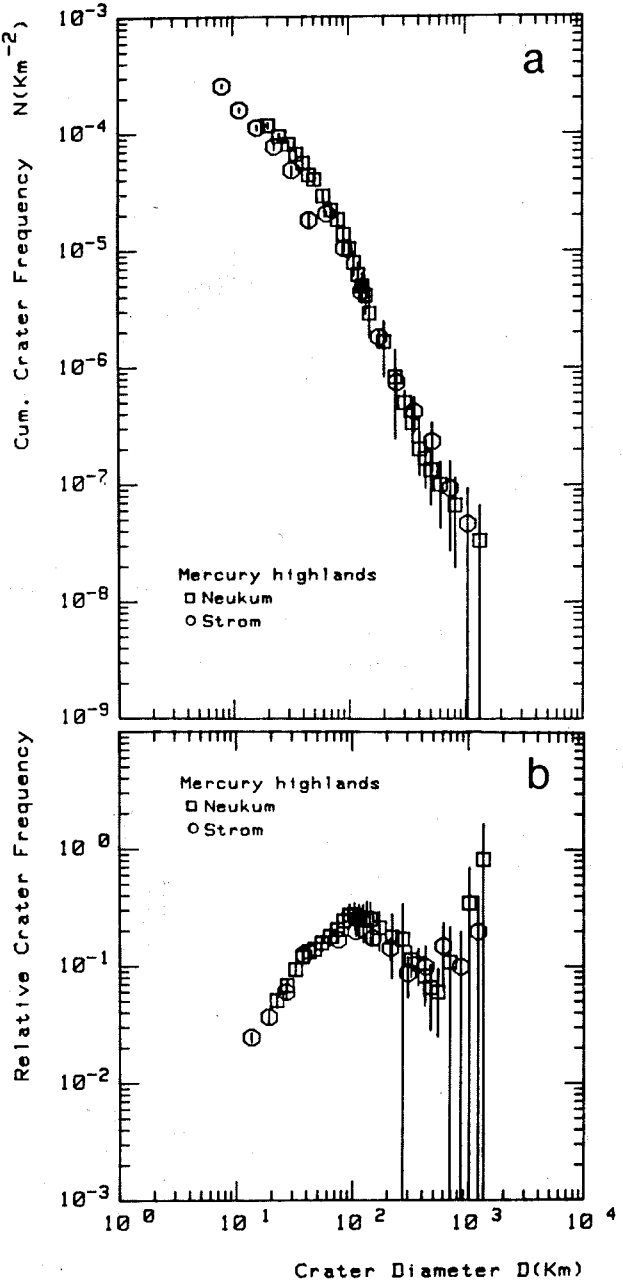

Fig. 1. Crater size-frequency distributions for the Mercurian highlands from two independent data sets of Neukum and Strom. The cumulative plot is shown in (a) and the relative plot in (b).

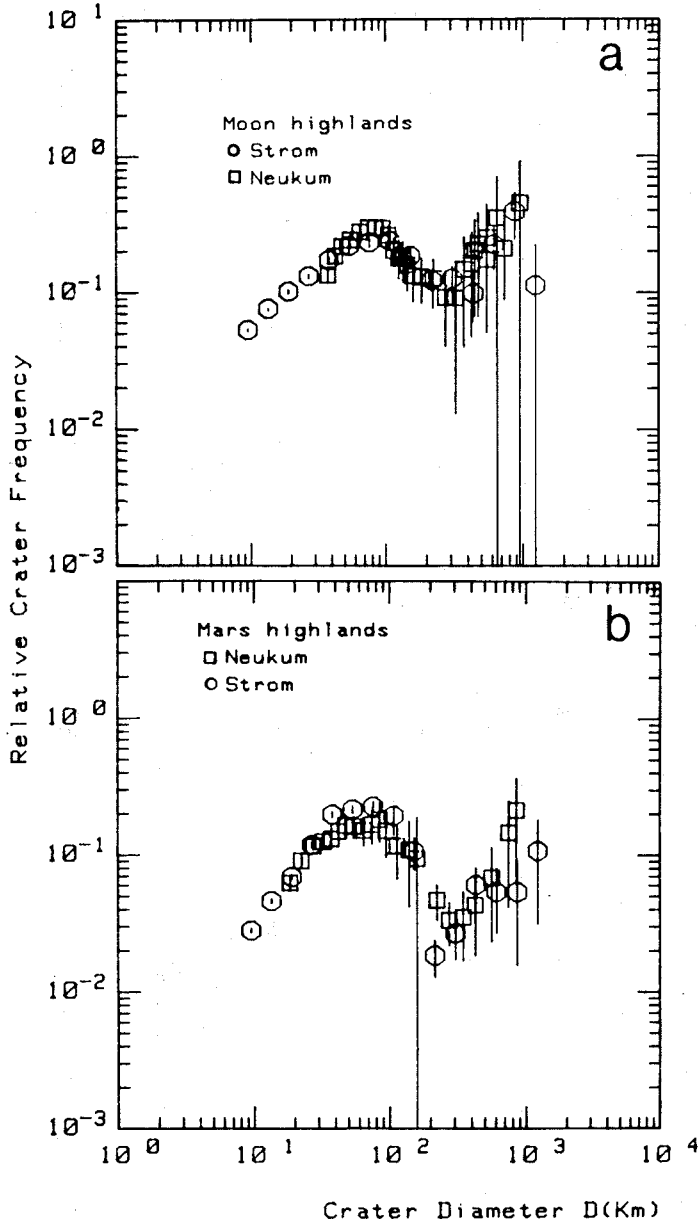

Fig. 2. "R" plots of the crater size-frequency distributions for the lunar highlands(a) and the Martian highlands (b) from two independent data sets of Neukum and Strom.

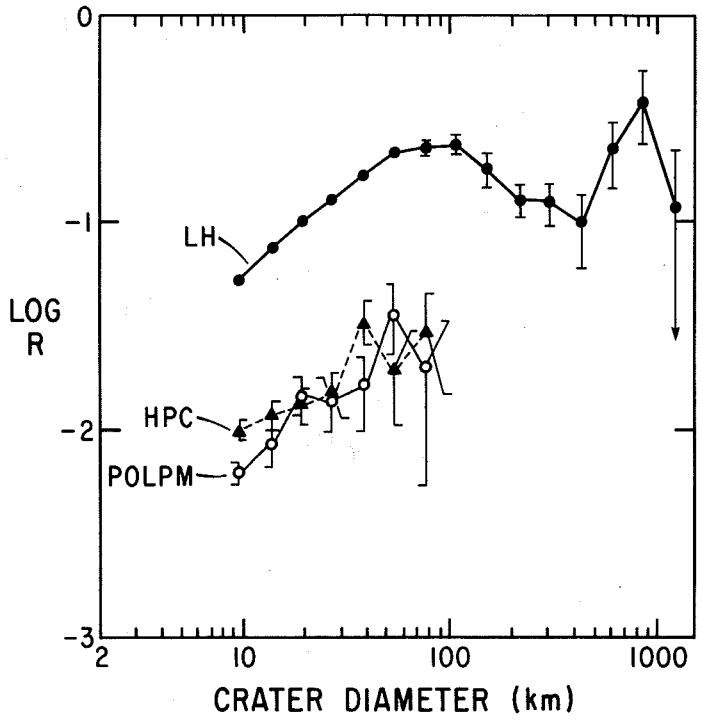

Fig. 3. Comparison of the crater size-frequency distributions of the lunar highlands (LH) with the post-Caloris crater population (HPC) and the post-Orientale population from which is subtracted the post-lunar mare crater population (POLPM). The shapes of the curves are similar over the same diameter range. See text for explanation.

nated by the largest craters (basins). There is not a unique crater density at which saturation occurs. It depends on the production function, and, in general, the shorter the dynamic range, the higher the density at which saturation occurs. One of the most important conclusions from the simulations is that the *observed size-frequency distributions on the most heavily cratered surfaces closely resemble their production size-frequency distributions, even if they are at or near saturation density.*

This latter result is supported by comparisons between crater populations on moderately cratered production surfaces and those on heavily cratered surfaces. Moderately cratered surfaces (surfaces with crater densities greater than that on the lunar maria and less than that in the highlands) show a crater size-frequency distribution that is essentially identical to that of the lunar highlands over the same diameter range of 8 to approximately 60 km. Such a population is found on the Orientale basin and continuous ejecta blanket (Fig. 3). This crater population represents the accumulation of impacts from the time of formation of the Orientale basin through the post-mare epoch up to the present

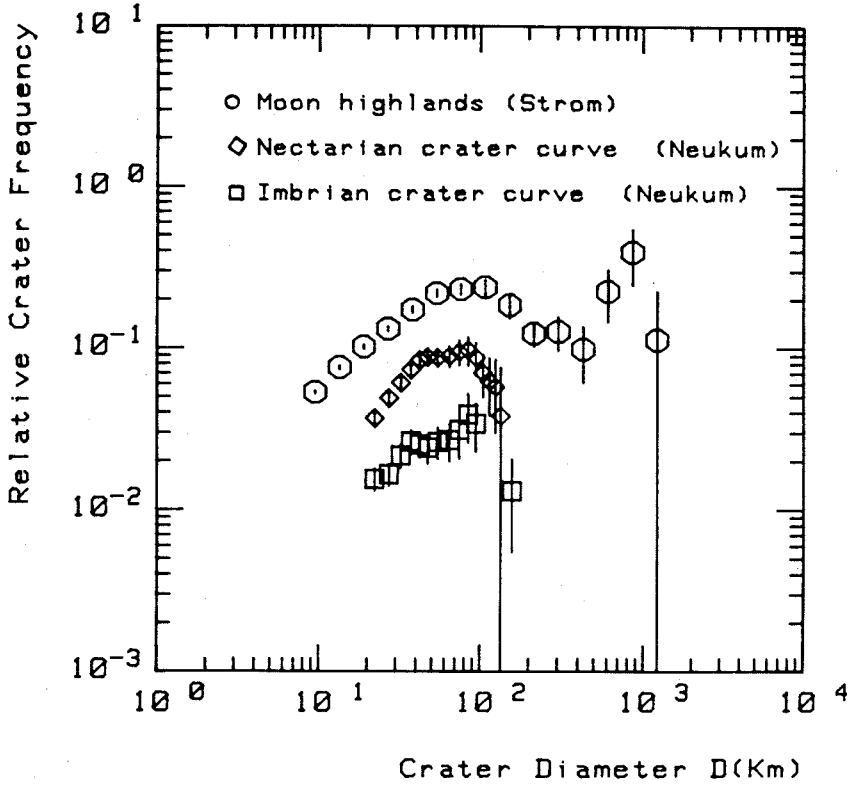

Fig. 4. "R" plot of the crater size-frequency distributions for the lunar highlands, and Nectarian- and Imbrian-aged craters. All size distributions have a similar shape but at different crater densities.

time. The Orientale impact is estimated to have occurred about 3.8 Gyr ago (Wilhelms 1984). The crater population formed between the Orientale impact and the emplacement of most of the lunar maria can be estimated by subtracting the post-mare population from the post-Orientale population normalized to the counting area on Orientale (Strom 1977). This post-Orientale/pre-mare population has a size-frequency distribution very similar to that of the lunar highlands (Fig. 3). The post-Caloris plains crater population on Mercury also has a crater density and size-frequency distribution very similar to the post-Orientale population (Fig. 3). Imbrian- and Nectarian-aged craters also have size-frequency distributions similar to that of the average lunar highlands (Fig. 4). The similarity between the production populations on moderately cratered production surfaces and the lunar highlands strongly suggests that the highlands crater population is basically the production population.

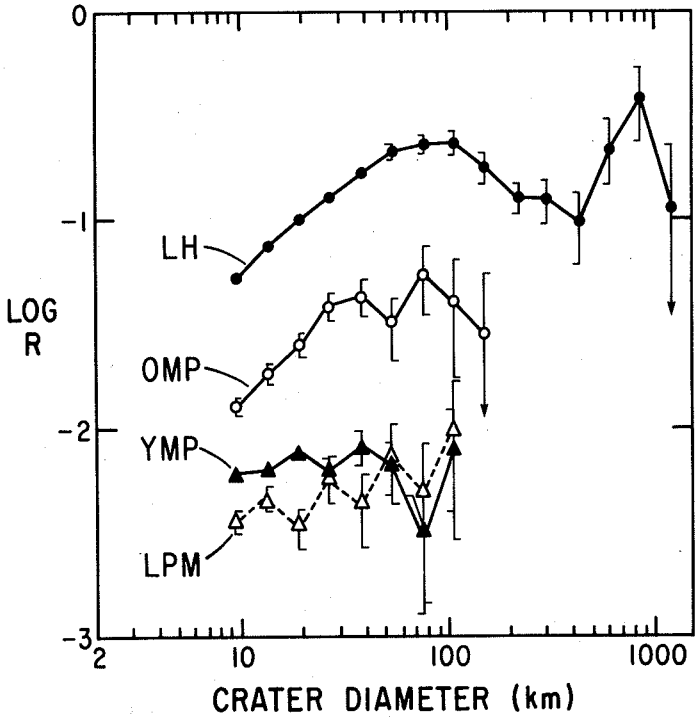

Fig. 5. "R" plot of the crater size-frequency distributions for the lunar highlands (LH), old Martian plains (OMP), young Martian plains (YMP), and the lunar post-mare (LPM) crater populations. The lunar highlands and old Martian plains crater populations are the same, but the young Martian plains and lunar post-mare populations are different at the chi-squared 99% confidence level.

On the Moon and Mercury, crater densities on these moderately cratered regions are relatively low or the counting areas are relatively small or both, so that the crater statistics are rather uncertain at diameters larger than about 40 km. Mars, however, has vast areas of plains which have a variety of ages. The number of craters between about 8 and 60 km diameter on these surfaces is large enough to provide good statistics with rather small uncertainties. On moderately cratered plains units the crater population is very similar to that of the lunar highlands (Fig. 5), again indicating the lunar highlands population is basically a production population.

The authors disagree between themselves about the crater population on the lightly cratered regions of the Moon (maria) and Mars (younger plains). One of us (G. Neukum) believes the size-frequency distribution is similar to the highlands population, while the other (R. Strom) believes it is significantly different. Neukum bases his belief on data consisting of craters interpreted to be of Erastothenian and Copernican age, while Strom includes all craters

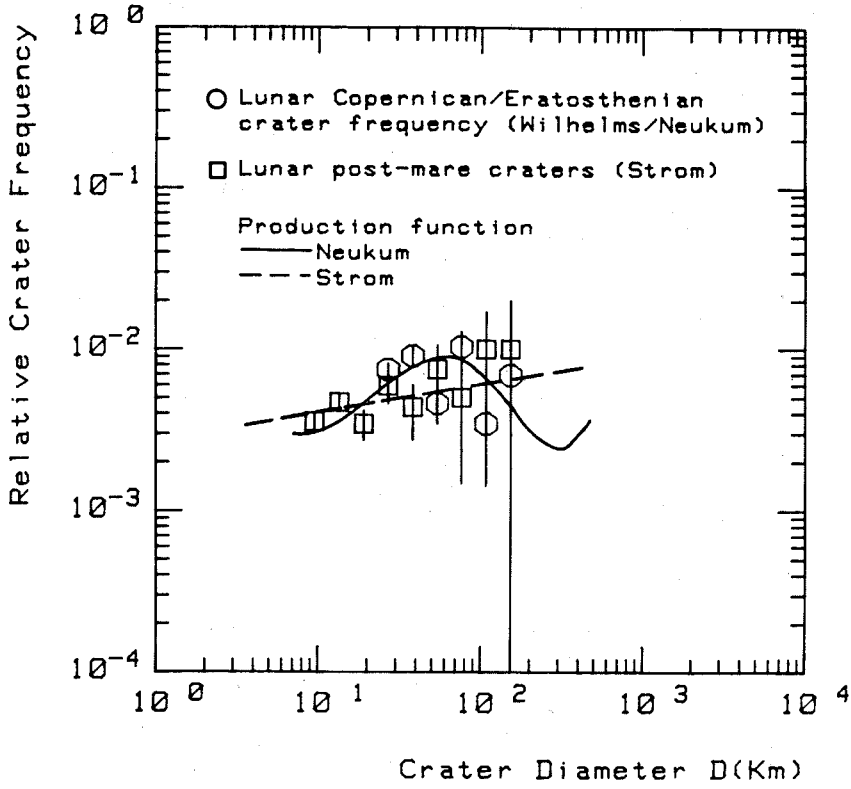

Fig. 6. Comparison of data sets for lunar post-mare and Eratosthenian plus Copernican craters. Also given are functions as advocated by Neukum and Strom, respectively. Here the authors disagree in interpretation. Neukum believes the production function is the same as for older populations as in Fig. 7 (see below), whereas Strom believes it has changed as in Fig. 5.

superimposed on the lunar maria and the younger Martian plains in his data. Chi-squared statistical tests of Strom's data indicate that the post-lunar mare population is different from that in the highlands at the 99% confidence level (Woronow et al. 1982; Strom 1977), and that the young post-Martian plains population is different at the 99.99% confidence level (Barlow 1987). These data are presented in Figs. 5 and 6, and the readers should judge for themselves the merits of the two interpretations. It should be noted, however, that this difference in interpretation is not central to the main issue of the heavily cratered terrains addressed in this chapter.

The question of whether or not the highlands crater populations on the Moon, Mars and Mercury have been modified by geologic processes is another important issue. There is little doubt that compared to the Moon there has been a loss of craters less than about 50 km diameter by geologic pro-

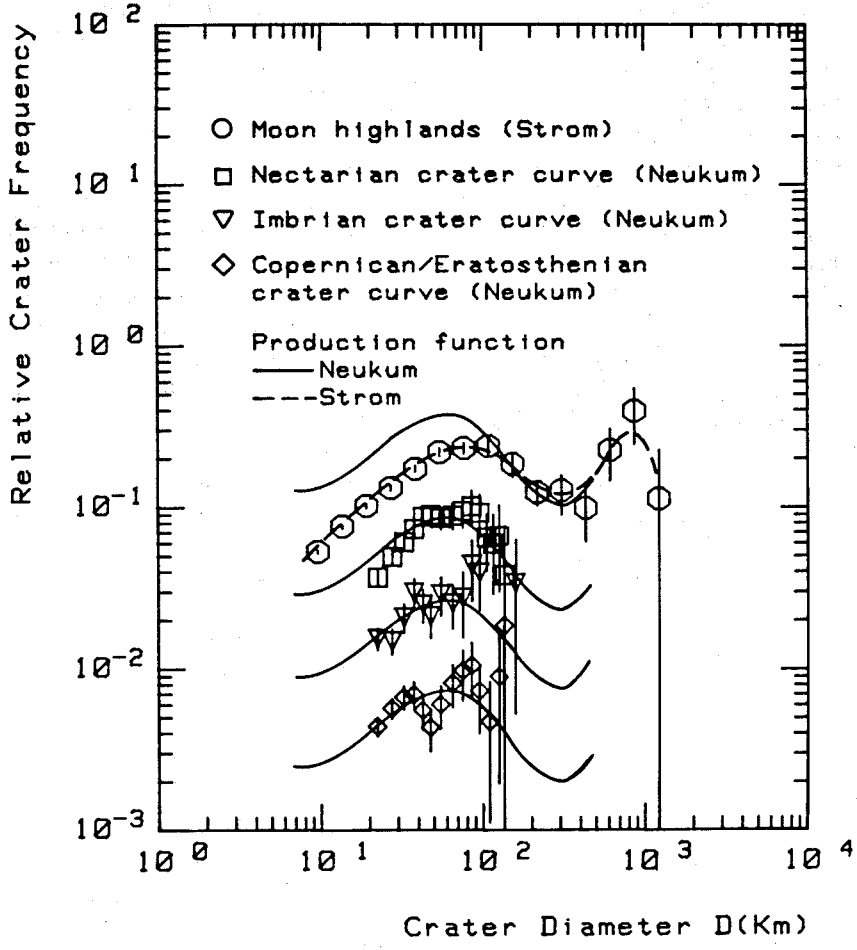

Fig. 7. Relative crater frequency plots of data from the lunar highlands, Nectarian-aged, Imbrian-aged, and Eratosthenian-aged surfaces. The highland data (Strom) are given in $\sqrt{2}$ intervals. The other data (Neukum) are given in much finer binning in order to bring out the structure of the distributions over the more limited size range better. These data have been smoothed by a floating average procedure to take out some of the statistical noise. Production functions are given in comparison. There is a slight disagreement of the authors in the interpretation of the data: Strom believes the lunar highland data totally reflect the production function for Imbrian to pre-Nectarian (highlands) ages, whereas Neukum believes that the production function as given here is not totally reflected in the highlands data but that the highlands distribution suffered some loss of craters (factor of 2 to 3) at sizes < 50 to 100 km from cratering and noncratering processes.

cesses on Mercury and Mars. This is discussed in Sec. III. The lunar highlands population at diameters greater than about 8 km must closely match the production population because the population index between 8 and about 50 km diameter is essentially the same as that for the production populations on moderately cratered areas of the Moon, Mars and Mercury. Between these diameters, it is virtually identical to Neukum's "ideal production population." This does not preclude the possibility that a portion of the smaller lunar crater population has been erased by the cratering process, although the Monte Carlo computer simulations by Woronow (1977) and Chapman and McKinnon (1986) do not show this. Large basin-forming events will obliterate all smaller craters over large areas. These areas are then recratered by smaller impacts which build up the crater density. The production distribution for these small craters is retained, although the crater density could be lower than that before the basin-forming events. Neukum's ideal production population has attempted to take this into account by increasing the crater density at diameters less than about 100 km while still preserving the observed production distribution (Fig. 7).

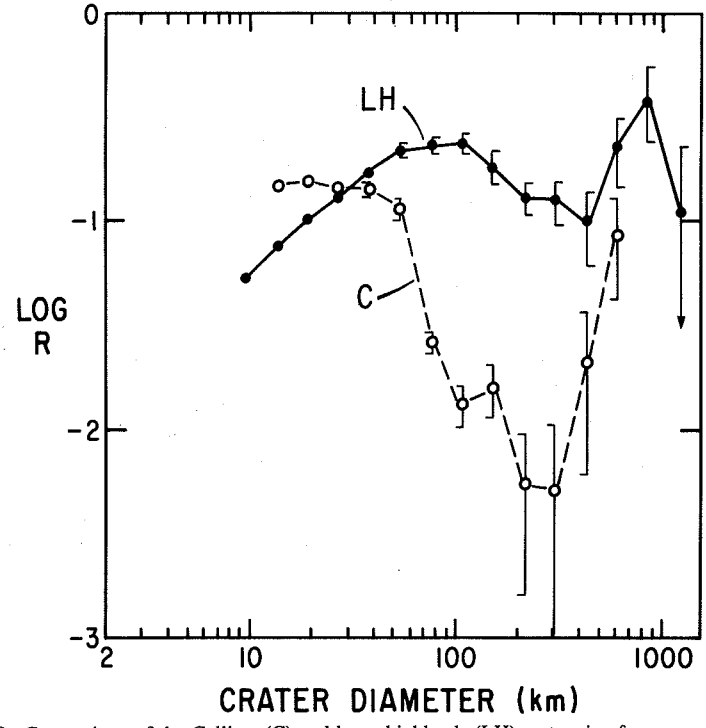

Fig. 8. Comparison of the Callisto (C) and lunar highlands (LH) crater size-frequency distributions. The crater populations are significantly different.

On Ganymede and Callisto the crater population shows a severe paucity of craters larger than about 60 km compared to the heavily cratered surfaces in the inner solar system (Fig. 8). This paucity of large craters has been attributed to obliteration of larger craters by viscous relaxation in ice (see, e.g., Passey and Shoemaker 1982; Shoemaker and Wolfe 1982). However, simulations by Woronow and Strom (1981), Chapman and McKinnon (1986) and Strom (1987*a*), and statistical tests by Gurnis (1987) show that this cannot be the case. These simulations reproduce the observed Callisto crater population using a lunar-highlands production function and incorporate diameter-dependent crater obliteration to simulate viscous relaxation. The resulting spatial distribution of craters is very nonuniform, exhibiting prominent holes where relatively recent large craters once existed. This is very different from what is observed on Callisto, where the spatial distribution of craters is quite uniform.

The main conclusion from computer modeling, simulations and observations of production populations on moderately cratered regions, is that the observed crater size-frequency distribution in the heavily cratered terrains on the inner planets (particularly the Moon) and at Jupiter are close to the initial production populations.

III. THE CRATERING RECORD AND GEOLOGIC PROCESSES

The age of Mercurian intercrater plains relative to the heavily cratered terrain has important implications for the early history of Mercury. The Mercurian highlands have a crater size-frequency distribution and density similar to that of the lunar and Martian highlands (Fig. 9). All show a highly structured curve with multiple distribution functions. The similar size-frequency distributions strongly suggest that the heavily cratered surfaces representing the period of late heavy bombardment in the inner solar system were the result of a single family of objects in heliocentric orbits. One difference between the lunar and Mercurian crater curves is that at diameters less than about 40 or 50 km diameter, Mercury shows a significant paucity of craters compared with the Moon (Fig. 9). Trask (1975) and Oberbeck et al. (1977) suggested that the Mercurian crater curve more closely represents the true crater production population analogous to a lunar highland curve from which widely distributed basin secondaries have been subtracted. However, it is much more likely that the paucity of craters on Mercury resulted from the obliteration of a fraction of craters by emplacement of intercrater plains (Strom 1977). Intercrater plains on Mercury are the major terrain type and cover a much larger fraction of the highlands than similar deposits cover on the Moon. They have surely been responsible for the obliteration of a portion of smaller craters since images show large craters embayed and partially buried by intercrater plains (Fig. 10). The Martian crater curve also shows a similar paucity of small craters relative to the Moon (Fig. 9) which must be due to plains formation in the Martian uplands and to eolian erosion. Furthermore, the post-Caloris crater

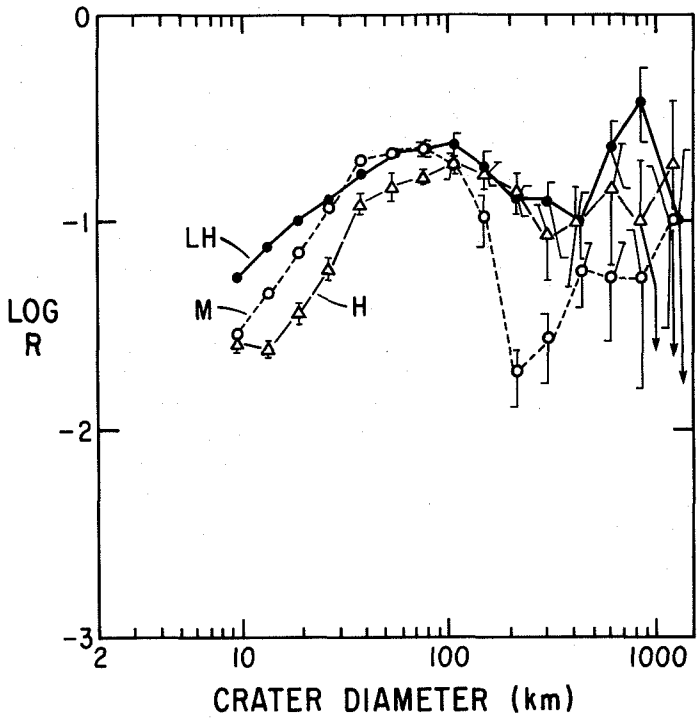

Fig. 9. "R" plot comparing the size-frequency distributions of the lunar highlands (LH), Mercurian (H), and Martian (M) highlands. The paucity of craters less than about 40 km on Mercury and Mars compared to the Moon is probably the result of crater obliteration by intercrater plains emplacement (see also Fig. 10).

size distribution must be in production and it is essentially identical to that of the lunar highlands, i.e., there is no paucity of smaller craters (Fig. 3). All of these observations strongly suggest that the paucity of smaller craters on Mercury's heavily cratered surface compared to the Moon is due to obliteration by intercrater plains emplacement. Intercrater plains show an abundance of craters less than about 15 km diameter that are largely secondary craters from craters in the heavily cratered terrain. Therefore, some of the intercrater plains are older than craters formed during the period of late heavy bombardment. This, together with the evident obliteration of craters by intercrater plains emplacements, strongly implies that intercrater plains formed *during* the period of late heavy bombardment. Leake (1982) and others have reached similar conclusions from stratigraphic studies. If the intercrater plains are volcanic in origin (Strom 1984; Leake 1982), then Mercury experienced much more volcanic activity during the period of late heavy bombardment than did the Moon.

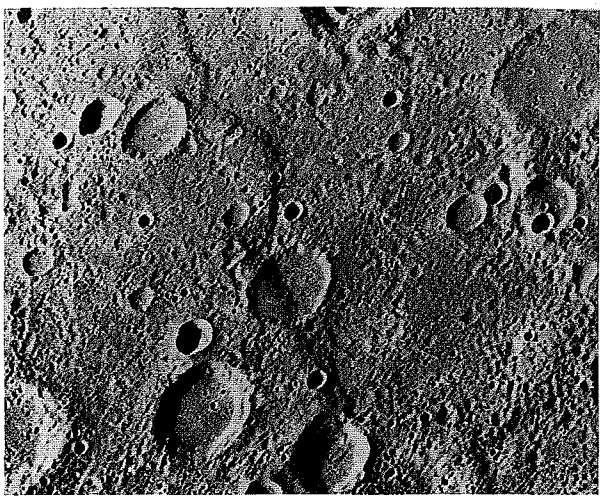

Fig. 10. Mariner 10 image of the intercrater plains in the Mercurian highlands. The large crater (70 km diameter) in the upper right-hand corner has been embayed by intercrater plains.

The crater population superposed on the smooth plains within and surrounding the Caloris basin has a size-frequency distribution that is essentially identical to that of the lunar highlands over the same diameter range of 8 to ~ 60 km (Fig. 3). The crater density of the post-Caloris population is about 10 times less than the Mercurian and lunar highlands, indicating that the smooth plains are relatively young. However, the post-Caloris population has a crater density about 5 times greater than the post-lunar mare crater population. It also has the same size distribution and crater density as the post-Orientale/pre-mare crater population (Fig. 11 in Strom 1977). The post-Orientale/pre-mare population is that which is superposed on the lunar Orientale basin and ejecta blanket from which is subtracted the post-mare population normalized to the area counted on Orientale. It therefore represents the time horizon between the Orientale impact and the emplacement of the lunar maria. The estimated age of the Orientale basin is about 3.8 Gyr (Wilhelms 1984). The similar shapes of the size-frequency distributions (lunar and Mercurian highlands, and post-Caloris and post-Orientale) indicate that the majority of Mercury's smooth plains were formed during, but near the end, of the period of late heavy bombardment.

If the intercrater and smooth plains are volcanic, then the cratering record suggests they were both emplaced early in Mercury's history during the period of late heavy bombardment. In fact, the formation of intercrater plains and smooth plains may not represent two distinct plains-forming episodes. Instead they may represent a more or less continuous period of plains formation lasting a shorter period of time than lunar volcanism. Volcanism may have lasted for a shorter period of time on Mercury than on the Moon because cooling of

the lithosphere and the large iron core produced global compression which closed off magma conduits and inhibited surface volcanism earlier on Mercury than on the Moon.

IV. ABSOLUTE TIME SCALES ON THE MOON AND MERCURY

The only reliable way of determining absolute surface ages is by radiometric age dating of returned samples. To date, only samples from the Earth, the Moon and meteorites have been dated in this way. One class of meteorites, the SNC meteorites, probably originated from Mars, but the location on Mars from which these meteorites came is very uncertain.

Absolute ages of planetary surfaces can be derived from crater statistics provided the cratering rate as a function of time, or the integrated impact rate as a function of absolute surface age is known. The cratering rate depends on the origin (orbital elements) of the impacting objects. For example, objects in planetocentric orbits will have a much greater impact rate on satellites than objects in heliocentric orbits. The origin of the objects responsible for the period of late heavy bombardment in the inner solar system is discussed in the following section. From the similarities of the crater population at Mars, the Moon and Mercury and lateral shifts between the crater curves, it is concluded that the objects were in heliocentric orbits confined to the inner solar system. If this is the case, then the impact rate would have been roughly similar at the Moon and Mercury and the end of late heavy bombardment would have occurred at about the same time on each body. On Mars, the end of late heavy bombardment by accretional remnants could have been extended by about 1 Gyr, according to Wetherill (1977).

It is also possible that the end of late heavy bombardment could have been extended on Mercury compared with the Moon if there was a population of potential Mercury-specific impactors ("vulcanoids") in orbits nearer to the Sun than Mercury (Leake et al. 1987). However, searches from 1902 to 1981 for such objects that should still be present have proved negative (Leake et al. 1987). These searches have shown that there is no appreciable population of vulcanoids larger than 50 km diameter orbiting interior to Mercury, although smaller objects may be present. The authors believe that the cratering record representing the period of late heavy bombardment on Mercury cannot have been due to hypothetical vulcanoids because the size-frequency distribution is similar to that on the Moon and Mars, and because lateral shifts in crater curves between the Moon and Mercury indicate higher impact velocities on Mercury than the Moon. The similar crater curves indicate that the same family of objects was responsible for the period of late heavy bombardment on the Moon, Mercury and Mars. Whether vulcanoids would have the same size distribution is highly problematical. Vulcanoids would have much lower im-

pact velocities on Mercury than objects impacting both Earth and Mars. Therefore, the ratio of Mercurian to lunar impact velocity should be less than 1 rather than 1.37 to 2.18 as observed (see Sec. V below).

Although we believe that the cratering rate and end of heavy bombardment at Mercury were similar to that at the Moon for the reasons given above, the reader should be aware that certain assumptions are required to derive the absolute ages that follow. The first assumption is stated above and the other is that the Caloris basin formed at the end of the period of late heavy bombardment 3.85 Gyr ago. If the age of the Caloris basin is not 3.85 Gyr, then the chronology and derivation of absolute ages is directly affected. For the assumed lunar-like time dependence of the Mercurian impact rate, there is about 100 Myr age difference for every factor of two in crater frequency. If, for example, the Caloris basin formed 3.95 rather than 3.85 Gyr ago, then all other crater retention ages would be shifted to older ages by 100 Myr. Stated another way, any crater frequency would have to be a factor of two lower to yield the same as for Caloris at 3.85 Gyr. If the impact probability decreased rapidly with decreasing cratering rate (a factor of ~ 2 per 100 Myr) during the period of late heavy bombardment, then an uncertainty of about 100 Myr for the age of Caloris occurs. Hence, uncertainties greater than about 100 Myr in the derivation of absolute crater retention ages from this model appear unlikely.

If a surface is saturated many times over, then the crater frequencies cannot be used to determine absolute ages of these surfaces. However, we believe that the highland surfaces of the terrestrial planets are still in production although they may be close to saturation. It should be noted that if these surfaces were saturated many times over and the Caloris basin is about 3.8 Gyr old, then the highland surfaces would be as old or older than the age of the solar system.

The method to achieve relative and absolute age determination from crater statistics was developed for the Moon by different groups concentrating on different aspects (see, e.g., Öpik 1960; Shoemaker et al. 1962; Baldwin 1964,1971; Hartmann 1965,1966; Soderblom 1970; Neukum 1971,1981, 1982, 1983; Neukum and Wise 1976). In order to derive relative or absolute ages for a specific surface unit, it is necessary to verify by careful examination of the imagery and precise measurement that (1) a production density can be measured; (2) the structure to be dated is really one homogeneous geologic unit (no or negligible resurfacing in terms of destruction of craters of the population measured); (3) only superimposed craters and no relic or ghost craters from an underlying older unit are measured; (4) secondary craters and volcanic craters are eliminated; (5) the area of measurement is determined accurately; and (6) the size of craters is measured with highest possible precision since the exponential size-frequency distribution dependence amplifies small errors in diameter as large errors in crater density per unit area.

The relationship between a crater production size-frequency distribution and age (termed crater retention age) is as follows: The crater population on one planet approximately represents the mass-velocity distribution of the impactors responsible for the cratering record. Under the assumption of mean impact velocity, a meteorite population (i.e., the impactors) of the mass distribution $n(m,t)$ in the mass interval $(m, m+\mathrm{d}m)$ causes a crater size-frequency distribution $n(D,t)$ in the crater diameter interval $(D, D + \mathrm{d}D)$ for a specific exposure time t. The function $n(D,t)$ is termed differential distribution (number per unit area per diameter at time t). The relationship between differential distribution and differential cratering rate (number per unit area per diameter per time at time t) is given by:

$$n(D,t) = \int_o^t \varphi(D,t')\mathrm{d}t' \tag{1}$$

where t is the exposure time with respect to the age of the crater population ($t > 0$). The cumulative crater frequency $N(D,t)$ (number per unit area of all craters with diameters equal to or larger than D and which were formed during exposure time t) is given by

$$N(D,t) = \int_D^\infty n(D,t)\mathrm{d}D' = \int_D^\infty \int_o^t \varphi(D',t')\mathrm{d}D'\mathrm{d}t'. \tag{2}$$

Note that this is in the continuous approximation; in reality, it is the sum of discrete numbers. The cumulative crater rate $\phi(D,t)$ is given by

$$\phi(D,t) = \int_o^t \phi(D,t')\mathrm{d}t' \text{ or } \phi(D,t) = \partial N(D,t)/\partial t. \tag{3}$$

The function $\varphi(D,t)$ can be separated into a function $g(D,t)$ that reflects the underlying crater size distribution and into a function $f(t)$ that reflects the general functional dependence of cratering rate on time. Therefore one can write

$$\varphi(D,t) = g(D,t) \cdot f(t) \tag{4}$$

or

$$\phi(D,t) = \int_D^\infty g(D't)f(t)\mathrm{d}D' = G(D,t)f(t). \tag{5}$$

If the size distribution is not directly dependent on time (i.e., the diameter distribution is the same over the whole exposure time), then the function $\varphi(D,t)$ can be separated in

$$\varphi(D,t) = g(D)f(t) \tag{6}$$

and

$$n(D,t) = g(D) \int_o^t f(t')\mathrm{d}t' \tag{7}$$

or $n(D,t) = g(D)F(t)$ where $F(t) = \int_o^t f(t')\mathrm{d}t'$. The cumulative crater frequency then is

$$N(D,t) = \int_D^\infty \int_o^t g(D')\mathrm{d}D'\, f(t')\mathrm{d}t' = G(D)DF(t) \tag{8}$$

which is a production distribution.

The production crater frequencies $n(D,t)$ or $N(D,t)$ show the same value, respectively, for areas exposed for an equal length of time on one planet for the same crater diameter or diameter interval regardless of location on the planet, provided the impactor flux is isotropic and target material compositions have no influence. In this case, we find the simple relationship

$$N_1(D,t,)/N_2(D,t_2) = F(t_1)/F(t_2). \tag{9}$$

This means that the ratio of the crater production population frequencies on two areas (1 and 2) is directly proportional to the ratio of their functional dependence on time. From this relationship a relative age sequence of geologic units can be determined by direct comparison of their superimposed impact crater frequencies; i.e., the frequency of superimposed craters (per unit area) for a specific diameter or a specific diameter interval is a direct measure of relative age, termed relative crater retention age.

For direct extraction and comparison of relative ages of two or more units, it is necessary to measure in the same crater size range or, if that is not possible, to compare crater frequencies through application of the functional dependence of the production distribution (called standard or calibration distribution by Neukum and Wise [1976]) and to convert the measured frequencies in this way to the values which they would show at one and the same diameter if they could be measured there. The ideal production distributions for the Moon and Mercury were estimated over different crater sizes by a variety of authors and the results were synthesized by Neukum (1983) as

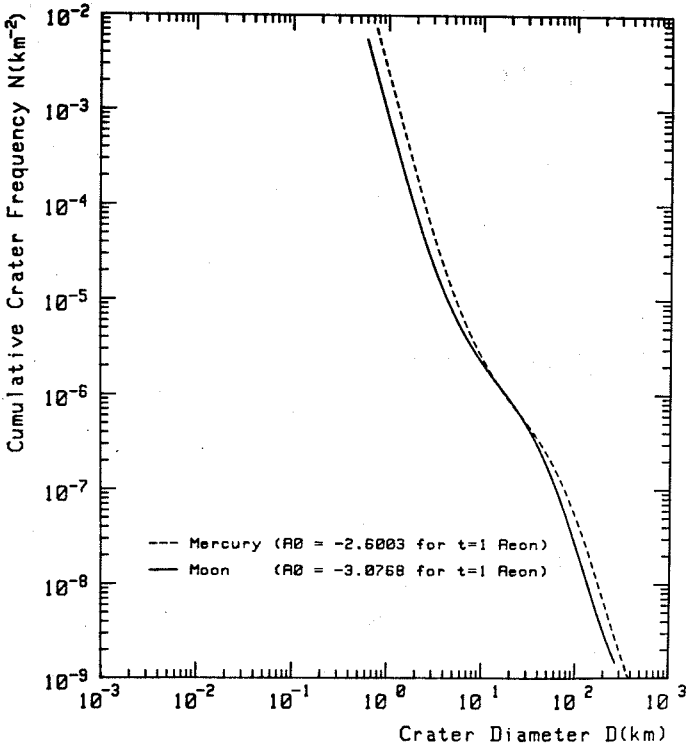

Fig. 11. Ideal cumulative crater size-frequency production distributions (polynomial of 11th degree) for the Moon and Mercury (figure after Neukum 1983).

shown in Fig. 11. The distributions are complex curves which cannot be approximated by simple power laws. The lunar and Mercurian production distributions as shown in Fig. 11 are directly related to each other and can be brought to coincide if one properly accounts for the difference in crater scaling due to factors like different impact velocity and gravity. The conversion from one planet to another along with the general relationships among the different terrestrial planets are summarized in Table 1.

The fact that two *different* values of crater frequency of the two planets at some diameter, or the *same* values at another diameter, may mean the same age of units on different planets is illustrated in Fig. 11 for the Moon and Mercury. The ideal cumulative production size-frequency distributions (calibration distributions) for both planets are given for the same age (t = 1 Gyr). Around D = 10 to 30 km, the size-frequency distributions fall almost upon each other, whereas the frequencies are quite different at smaller and larger diameters. This demonstrates that it is absolutely necessary to specify exactly the diameter or range of diameters in age determinations.

TABLE I

Conversion Factors for Crater Scaling on the Terrestrial Planets[a]

Object	V_{iP} (km s^{-1})	$(2GM_P/R_p)^{1/2}$ (km s^{-1})	g_P (cm s^2)	$U_{\infty P}$ (km s^{-1})	f_P	$F = f_P/f_M$	$\left(\frac{g_M}{g_P}\right)^{3/16}$	$\left(\frac{V_{ip}}{V_{iM}}\right)^{0.56}$	$D_p/D_M = \left(\frac{g_M}{g_P}\right)^{3/16} \times \left(\frac{V_{ip}}{V_{iM}}\right)^{0.56}$
Moon	14.1	2.38	162	13.90	1.03	1.00	1.000	1.00	1.00
Mercury	23.6	4.2	363	23.22	1.03	1.00	0.860	1.33	1.15
Venus	19.3	10.3	860	16.32	1.40	1.36	0.731	1.19	0.87
Earth	17.8	11.2	982	13.83	1.66	1.61	0.713	1.14	0.81
Mars	12.4	5.0	374	11.35	1.19	1.16	0.855	0.93	0.80

[a]Symbols have the following meaning:
D = crater diameter on the planet with gravitational acceleration.
$g_P = GM_P/R_P^2$ with M_P, R_P = planetary mass, planetary radius and $G = 6.67 \times 10^{-8}$ gravitational constant.
V_{iP} = impact velocity for projectiles of eccentricity $e = 0.6$.
$U_{\infty P}$ = relative velocity for projectiles on the border of gravitational sphere of action of planet.
$U_{\infty P} = (GM_\odot/1_{\odot P})^{1/2} (e^2 + e_P^2)^{1/2}$, $M_\odot$ = solar mass, e = eccentricity of projectile, e_P = eccentricity of planetary orbit, $1_{\odot P}$ = solar distance of planet.
$V_{iP} = (2GM_P/R_P + U_{\infty P}^2)^{1/2}$ = impact velocity = square root of the quantity consisting of square of escape velocity + square of relative velocity on the border of planet's gravitational sphere.
$f_P = (1 + 2GM_P/R_P\, U_{\infty P}^2)$ = focusing due to planet's gravitation.
Values for the Moon are indexed with M.
$D_P \propto V_{iP}^{0.56}/g_P^{3/16}$; $D_M \propto V_{iM}^{0.56}/g_M^{3/16}$; $D_P/D_M = (g_P/g_P)^{3/16} (V_{iP}/V_{iM})^{0.56}$.
$F = f_P/f_M = (1 + 2GM_P/R_P U_{\infty P}^2)/(1 + 1GM_M/R_M U_{\infty} M)$.
Subscript P = planet; subscript M = Moon.

The Mercurian cumulative crater production size-frequency distribution can be approximated by a polynomial of 11th degree as shown by Neukum (1983):

$$\begin{aligned}
\mathrm{Log}N &= a_0 + a_1(\log D) + \cdots + a_{11}(\log D)^{11} \\
a_1 &= -3.6712 \quad a_7 = 3.2493 \times 10^{-2} \\
a_2 &= 0.2946 \quad a_8 = 1.1737 \times 10^{-2} \\
a_3 &= 0.7630 \quad a_9 = -1.9272 \times 10^{-3} \\
a_4 &= 0.1620 \quad a_{10} = -5.4447 \times 10^{-4} \\
a_5 &= -0.2379 \quad a_{11} = 3.97 \times 10^{-5} \\
a_6 &= -8-8.1361 \times 10^{2}.
\end{aligned} \tag{10}$$

The coefficient a_0 is variable and contains the age dependence of the distribution. Some specific values as for the curves in Fig. 13 below are

$$\begin{aligned}
a_0 &= -5.6003 \text{ for } t = 0.001 \text{ Gyr} \\
a_0 &= -4.6003 \text{ for } t = 0.01 \text{ Gyr} \\
a_0 &= -3.6003 \text{ for } t = 0.1 \text{ Gyr} \\
a_0 &= -2.6003 \text{ for } t = 1.0 \text{ Gyr} \\
a_0 &= -1.9461 \text{ for } t = 3.4 \text{ Gyr} \\
a_0 &= -1.2669 \text{ for } t = 3.8 \text{ Gyr} \\
a_0 &= -0.1409 \text{ for } t = 4.2 \text{ Gyr}.
\end{aligned} \tag{11}$$

A surface unit on Mercury that is exposed to meteorite bombardment will show more and more craters in all sizes according to the functional diameter-dependence of the production distribution and according to the functional dependence on time with respect to cratering rate. N is proportional to 10^{a_0} for a specific fixed diameter. Therefore one will find, as illustrated in Fig. 12, that the calibration distribution will shift in the log$N$ direction with exposure time (with *no* shift in diameter direction) by the same amount at all diameters, directly related to the functional dependence of cratering rate on time.

The cratering rate dependence on time with respect to the dependence of the accumulated cratering record as a function of age (i.e., the cratering chronology) cannot directly be determined for Mercury presently, since no absolute age information for surface rock units is available. Therefore it currently is only possible to estimate the Mercurian cratering chronology by extrapolating the lunar cratering chronology to Mercury under certain assumptions as discussed earlier. There exist essentially two different methods of extrapolating the lunar chronology to Mercury:

1. The cratering rate at Mercury compared to that at the Moon is estimated from present-day observations and theoretical considerations on asteroidal and cometary bodies and from relevant impact probabilities (Hartmann 1977; Basaltic Volcanism Study Project 1981). The functional dependence of the Mercurian cratering rate on time is assumed to be the same as for the

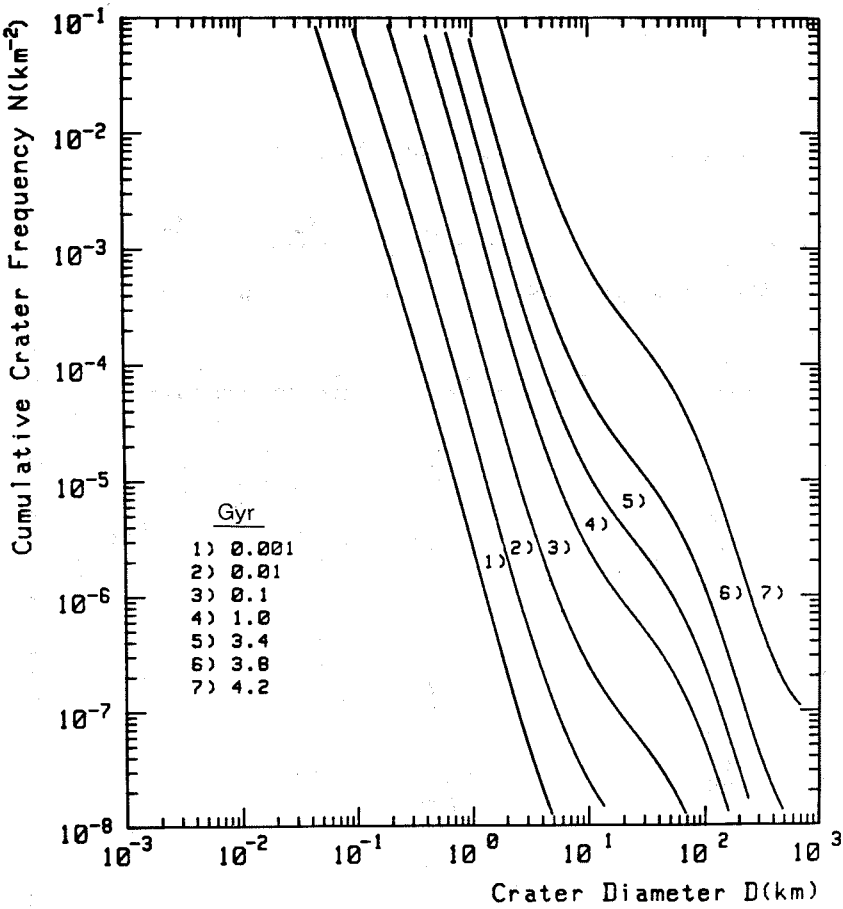

Fig. 12. Crater retention isochrons (polynomial of 11th degree) for Mercury. See text for explanation (figure after Neukum 1983).

Moon. Corrections for impact velocity, scaling and gravitational focusing effects are made similarly to our procedure in Table I.

2. Nothing is assumed about relative cratering rates. The functional dependence of the Mercurian cratering rate on time is assumed to be the same as for the Moon as in method (1). Specifically, it is assumed that the heavy bombardment that created the major basins on the Moon ended at the same time on Mercury; i.e., the age of the Imbrium or Orientale basin on the Moon (3.8 to 3.85 Gyr) is approximately the same as the age of the Caloris basin on Mercury (Neukum 1983). Caloris is set at 3.85 Gyr. Corrections for impact velocity, scaling and gravitational focusing effects are applied as given in Table I.

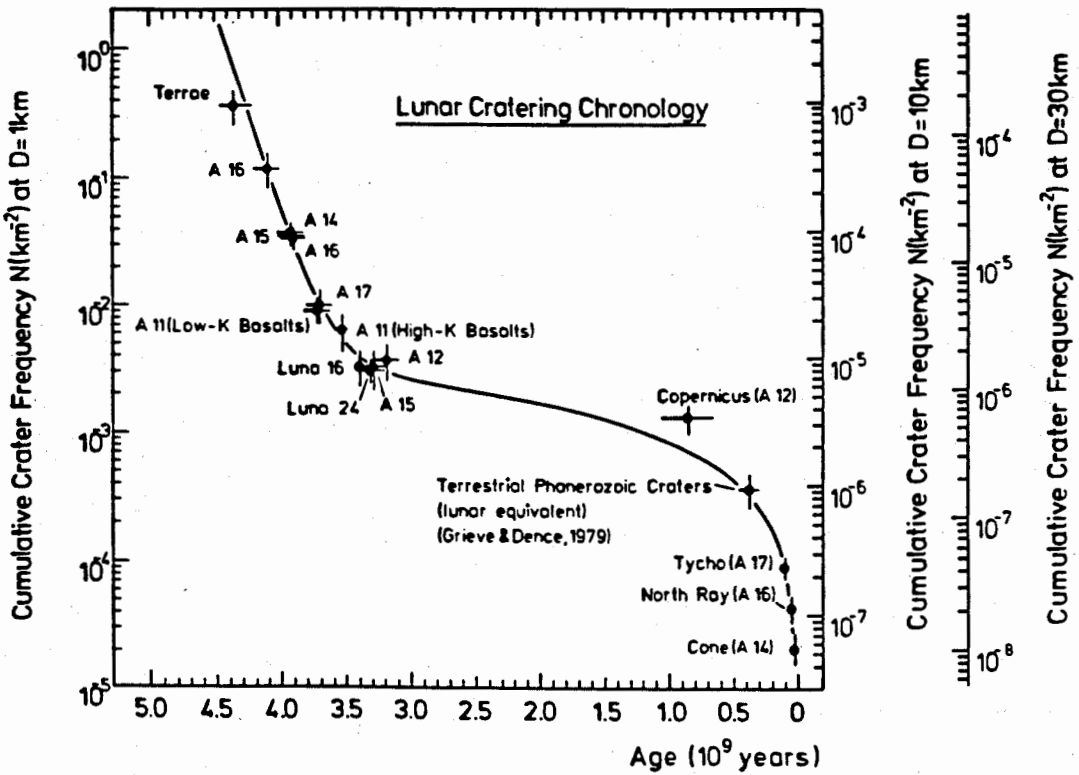

Fig. 13. Cumulative crater frequencies for various lunar surfaces dated from returned lunar samples.

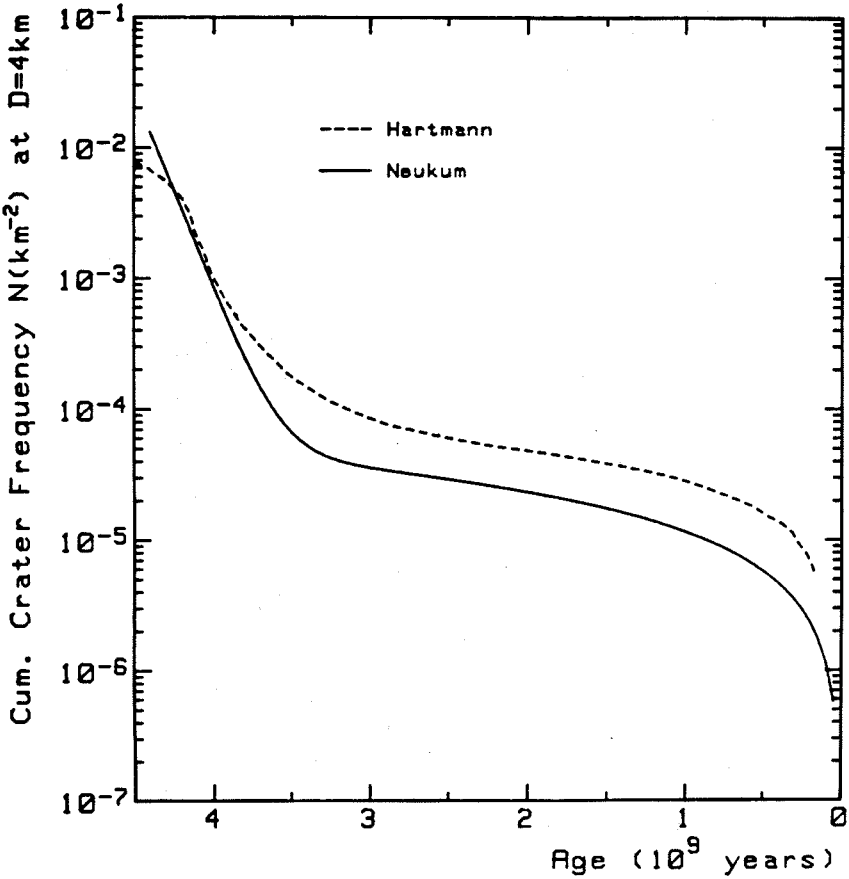

Fig. 14. Comparison of the lunar cratering chronologies derived by Neukum and Hartmann. See text for discussion.

The procedure described as method (2) is followed here.

Important in the derivation of the Mercurian cratering chronology is the quality of the lunar cratering chronology data. In our interpretation, we make use of the data by Neukum (1983) which are shown in Fig. 13. Hartmann's lunar data (Basaltic Volcanism Study Project 1981), shown in comparison in Fig. 14, lie systematically higher. The same is true for his Mercurian chronology curve. Application of Hartmann's curve to crater frequency data measured on Mercurian surface units would result in systematically younger ages. One major reason for the discrepancy between Hartmann's and Neukum's lunar chronologies is the difference in the data used for the determination of the chronology for ages < 1 Gyr. As discussed by Neukum (1983), Hartmann's data are based on a few scattered points with large error bars.

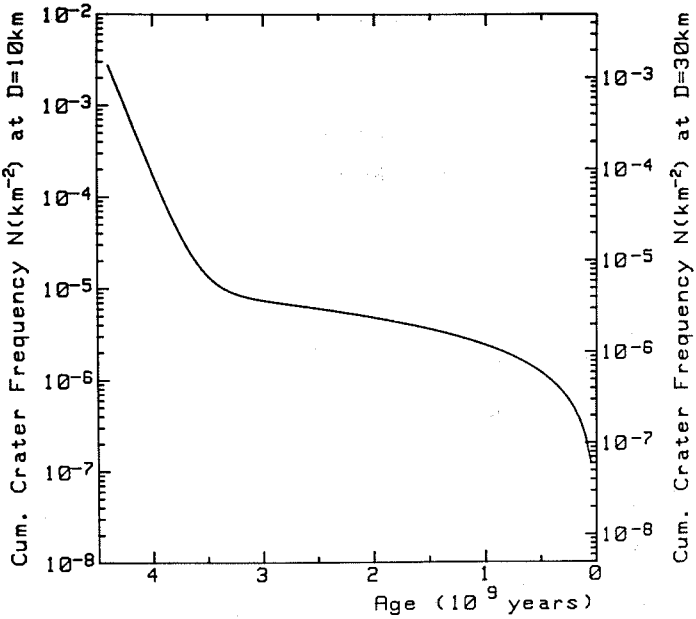

Fig. 15. Cratering chronology of Mercury derived by Neukum.

Our conversion of the lunar cratering chronology curve to the Mercurian case results in the dependence shown in Fig. 15. Numerically, the Mercurian cratering chronology in terms of cumulative crater frequencies at diameters D = 4 km, 10 km and 30 km reads:

$$N(D = 4\ km) = 1.37 \times 10^{-15}(e^{6.93t} - 1) + 2.10 \times 10^{-5}t \quad (12)$$

$$N(D = 10\ km) = 1.56 \times 10^{-16}(e^{6.93t} - 1) + 2.40 \times 10^{-6}t \quad (13)$$

$$N(D = 30\ km) = 3.16^{-17}(e^{6.93t} - 1) + 4.87 \times 10^{-7}t \quad (14)$$

where t is the age in units of 1 Gyr and N is the cumulative crater frequency per km^2.

The Mercurian cumulative crater frequencies at different diameters are related to each other through the Mercurian cumulative crater production size-frequency distribution as given in Figs. 11 and 12, and as approximated by the polynomial of 11th degree discussed above.

Absolute ages can be determined from crater statistics measured for specific Mercurian surface units in the following way:

1. Graphical determination: a value of N at a specific diameter is determined directly from the measured data or determined for a different reference

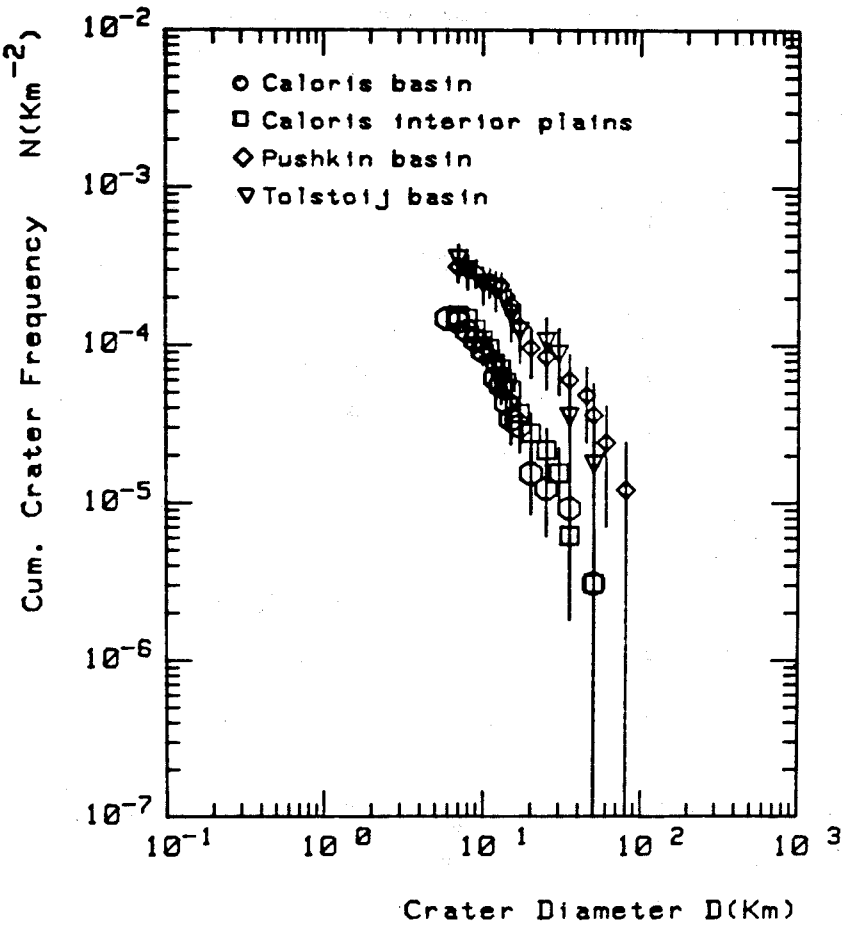

Fig. 16. Cumulative crater frequencies for Mercury's Caloris basin, Caloris interior plains, and the Pushkin and Tolstoij basins.

diameter (here 10 km or 30 km) through application of the Mercurian calibration distribution. The N value is introduced into the chronology graph (y-axis in Fig. 15) and the corresponding absolute crater retention age is read on the x-axis.

Numerical determination: a value of N for a specific diameter is computed by a least-squares fit of the calibration distribution to the measured data. This N value is introduced into the numerical expression of the Mercurian cratering chronology (as above) and the equation solved for t.

Crater frequency measurements for Mercurian highlands, basins and plains were conducted by Strom (1977), Leake (1982) and Neukum (1983)

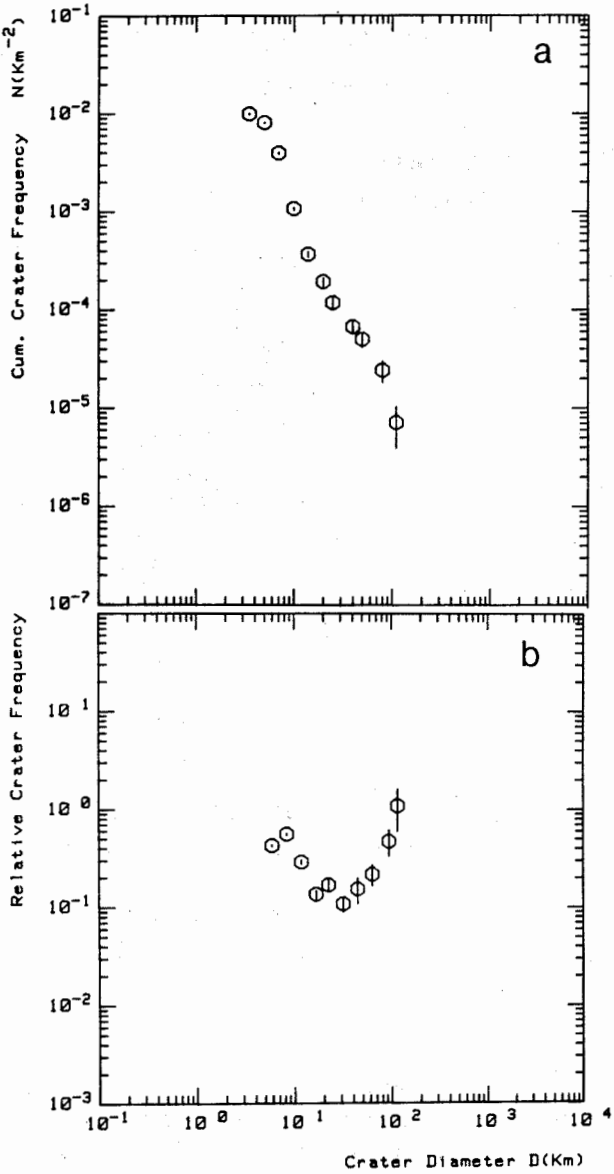

Fig. 17. Cumulative plot (a) and "R" plot (b) of the crater size-frequency distribution of the intercrater plains on Mercury.

TABLE II

Relative and Absolute Crater Retention Ages for Various Terrains on Mercury[a]

Area	Relative Crater Retention Age			Absolute Crater Retention Age (Gyr)
	$N(D = 4\text{km})\ \text{km}^{-2}$	$N(D = 10\text{km})\ \text{km}^{-2}$	$N(D = 30\text{km})\ \text{km}^{-2}$	
Highland	5.25×10^{-3}	5.99×10^{-4}	1.22×10^{-4}	4.18
Beethoven basin	1.34×10^{-3}	1.53×10^{-4}	3.10×10^{-5}	3.98
Chekhov basin	3.54×10^{-3}	4.04×10^{-4}	8.21×10^{-5}	4.12
Caloris basin	6.01×10^{-4}	6.85×10^{-5}	1.39×10^{-5}	3.85
Caloris mare (Interior)	6.01×10^{-4}	6.85×10^{-5}	1.39×10^{-5}	3.85
Dostoevskij basin	4.81×10^{-3}	5.49×10^{-4}	1.11×10^{-4}	4.17
Haydn basin	3.20×10^{-3}	3.65×10^{-4}	7.41×10^{-5}	4.11
Pushkin basin	3.02×10^{-3}	3.45×10^{-4}	7.00×10^{-5}	4.10
Raphael basin	3.23×10^{-3}	3.69×10^{-4}	7.49×10^{-5}	4.11
Tolstoij basin	2.33×10^{-3}	2.66×10^{-4}	5.39×10^{-5}	4.06
Intercrater plains				
Oldest	6.95×10^{-3}	7.93×10^{-4}	1.61×10^{-4}	4.22
Youngest	1.81×10^{-3}	2.06×10^{-4}	4.19×10^{-5}	4.02
Average	4.41×10^{-3}	5.03×10^{-4}	1.02×10^{-4}	4.15

[a]The errors of measurement are in all cases about $< \pm 30\%$ in N.

among others. Examples for the basins Tolstoij, Pushkin and Caloris are presented in Fig. 16 and for the highlands in Fig. 1a (as cumulative crater frequencies). Data for Mercurian intercrater plains are shown in Fig. 17a (cumulative frequencies) and 17b (relative frequencies). Application of the Mercurian calibration curve (Fig. 11) to the cumulative crater frequencies yields the relative crater retention ages as listed in Table II (for $D = 4$, 10 and 30 km). Application of the Mercurian cratering chronology as in Fig. 15 (or the numerical expression for it discussed earlier) results in the respective absolute crater retention ages (Table II). With the age of Caloris basin set at 3.85 Gyr, the Mercurian highlands fall at $\sim$ 4.2 Gyr on the average and the ages of the eight basins investigated fall between 4.2 Gyr and 3.85 Gyr.

The intercrater plains did not form at one point in time but during the whole period of heavy bombardment, the oldest plain having an average highland age, the youngest plain investigated having an age of $\sim$ 4 Gyr. The fill of Caloris (smooth plains) has an age indistinguishable from that of the Caloris basin (rim and ejecta blanket). This means the volcanic filling of the basin occurred soon after the formation of Caloris.

V. IMPLICATIONS FOR THE ORIGIN OF IMPACTING OBJECTS

The heavily cratered highland surfaces on the Moon, Mars and Mercury represent the period of late heavy bombardment which ended, at least on the Moon, about 3.8 Gyr ago. Each of these surfaces displays similar crater size-frequency distributions indicating that they were impacted by the same family of objects (Fig. 9). Since these objects apparently spanned the entire inner solar system distance from Mercury to Mars, they were probably in heliocentric orbits.

At Jupiter, the cratering record is different (Strom et al. 1981). On Callisto and the heavily cratered areas of Ganymede, the crater size-frequency distribution shows a severe paucity of craters greater than 50 km diameter and an overabundance of craters less than about 30 km in diameter compared with that on the heavily cratered surfaces in the inner solar system (Fig. 18).

One could imagine that when crater scaling parameters are taken into account, the size-frequency distribution of the projectiles might be similar for the terrestrial planets and Jovian crater population. If the Ganymede or Callisto crater curve (Fig. 8) could be shifted a factor of 2 to larger diameters by differences in the scaling parameters, it would match more closely the crater curve of the terrestrial planet highlands (Neukum 1983, 1985; Horedt and Neukum 1984). Strom (1987*a*), however, employed a modified Holsapple-Schmidt (1982) crater scaling law to recover the size-frequency distribution of the impacting objects using present-day short-period comet impact velocities and found that the disparity between the projectile size distributions was even greater than that between the crater size distributions. Chapman and McKinnon (1986) reached similar conclusions.

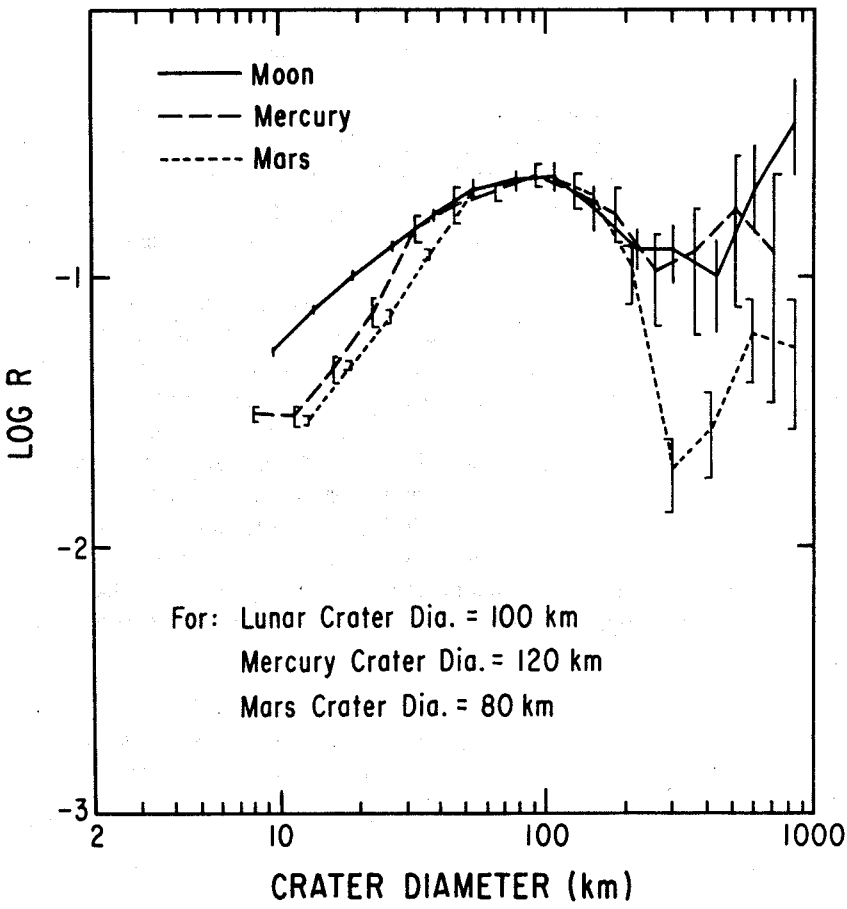

Fig. 18. The crater size-frequency distributions for the highlands of the Moon, Mars and Mercury (see Fig. 9) have been matched from about 40 km to 150 km diameter (the diameter range not affected by intercrater plains emplacement and having relatively good statistics). The lateral shifts in the curves require higher planet impact velocities with decreasing heliocentric distance (larger craters on Mercury and smaller ones on Mars compared to a given size crater on the Moon).

One can also analyze the problem dynamically by using the crater scaling law to solve for the impact velocity of a constant projectile diameter so that the crater curves more closely coincide. In this case, a given size projectile must make a crater twice as large on the Moon as on Callisto. The velocity V required to form a complex crater diameter D_r from a projectile diameter d is given by a modified Holsapple-Schmidt (1982) crater scaling law (Strom 1987*a*):

$$V = \left(\frac{D_q^{0.15} D_r^{0.85} g^{1/6}}{d^{1/1.2} Kc^{1/3} [1 - 0.095(1 - \sin A)]^{1/3}} \right)^3 \quad (15)$$

where D_q is the transition diameter from simple to complex craters, g is surface gravity, K is a coupling factor (~ 4.8), c is the ratio of projectile to target density, and A is the impact angle from the horizontal. The exponents of D_q and D_r are from Croft's (1985) empirical relationship D_e equals $D_q^{0.15} D_r^{0.85}$, where D_e is the excavation crater diameter. For simple bowl-shaped craters D_e is equal to D_r.

Since a high flux of comets early in solar system history has been proposed to account for the period of heavy bombardment throughout the solar system (Shoemaker and Wolfe 1982), we used a density of 1 g cm^{-3} for the projectile density. Table III lists the impact velocities required to form a 100 km crater on the Moon and a 50 km crater on Callisto for various comet diameters, i.e., the velocities required to shift the Callisto crater curve to match more closely that in the inner solar system. Also listed are the rms impact velocities for long-period and short-period comets on the Moon and Callisto. The required impact velocities are about 30 times greater on the Moon than on Callisto for a comet nucleus of similar size. This velocity difference is totally unrealistic for either short- or long-period comet orbits. The

TABLE III
Comet Impact Velocities to Form a 100 km Crater on the Moon and a 50 km Crater on Callisto for a Given Size Nucleus

Comet diameter (km)	Moon impact velocity (km s^{-1})	Callisto impact velocity (km s^{-1})
7	113.4	3.75
8	81.2	2.69
9	60.5	2.00
10	46.5	1.54
11	36.6	1.21
12	29.5	0.98
13	24.1	0.80
14	20.0	0.66
15	16.9	0.56
16	14.4	0.48
17	12.3	0.41
18	10.7	0.35
19	9.3	0.31
	Long-period comets rms impact velocity (km s^{-1})	Short-period comets rms impact velocity (km s^{-1})
Moon	52	20
Callisto	26	14

maximum difference between the rms impact velocity at the Moon and Callisto (long-period comets at the Moon and short-period comets at Callisto) is 38 km s^{-1}, or only a factor of 3.7 compared to the factor of 30 required to account for the differences in the cratering records between the two satellites. In fact, heliocentric objects with any combination of orbital elements are incapable of generating the impact velocity difference required to account for the disparity in the cratering curves in the inner solar system and at Jupiter. This strongly suggests that the objects responsible for the period of late heavy bombardment in the inner solar system were confined to the inner solar system, and that the objects impacting the Galilean satellites were in planetocentric orbits or predated the late heavy bombardment.

Additional evidence for this comes from a comparison of the cratering curves representing the period of heavy bombardment on the Moon, Mercury and Mars. Figure 9 shows the crater size-frequency distributions for the heavily cratered highlands of the Moon, Mars and Mercury representing the period of late heavy bombardment. They all have similar shapes except at diameters less than about 40 km where intercrater plains emplacement and erosion have modified the curves for Mercury and Mars as discussed earlier. However, at diameters between about 40 km and 150 km, where the curves are probably unaffected by erosion and the statistics are good, the curves are laterally displaced with respect to each other. They are displaced in such a manner that higher impact velocities are required at planets with smaller heliocentric distances, i.e., larger craters on Mercury and smaller craters on Mars compared to a given size crater on the Moon. This is consistent with objects in heliocentric orbits. There are uncertainties in the amount of displacement giving the best match of the curves, but the outside limits are as follows: relative to a 100 km crater on the Moon, the displacement is from 0 to 20 km larger on Mercury and 20 to 30 km smaller on Mars. The best fit is shown in Fig. 18 where for a 100 km crater on the Moon, the crater size on Mercury is 120 km and on Mars 80 km.

Equation (15) can be used to calculate the impact velocities required to form a given size crater for a constant size projectile on the Moon, Mercury and Mars, and from these velocities determine the impact velocity ratios, Mercury/Moon and Mars/Moon. The outside limits on the displacements give a Mercury/Moon impact velocity ratio between 1.37 and 2.18, and a Mars/Moon impact velocity ratio between 0.48 and 0.68. The best fit shown in Fig. 18 gives a Mercury/Moon impact velocity ratio of 2.18 and a Mars/Moon impact velocity ratio of 0.68.

The orbital elements (semimajor axes and eccentricities) and impact velocity ratios of impacting objects in heliocentric orbits can be derived from the equations for impact velocity. In simplified form, the impact velocity V_{ip} for a heliocentric object with a planet is:

$$V_{ip} = (U^2 + V_e^2)^{1/2} \tag{16}$$

where U is the encounter velocity of the object at infinity, and V_e is the escape velocity of the planet. For a heliocentric object impacting a satellite, the mean impact velocity V_{is} is:

$$V_{is} = (U^2 + V_{eo}^2 + V_{es}^2)^{1/2} \tag{17}$$

where V_{eo} is the escape velocity of the planet at the orbit of the satellite, and V_{es} is the escape velocity of the satellite.

Figure 19 is a plot of the comparison of the impact-velocity ratios of Mercury/Moon (a), and Mars/Moon (b), vs impactor semimajor axes from

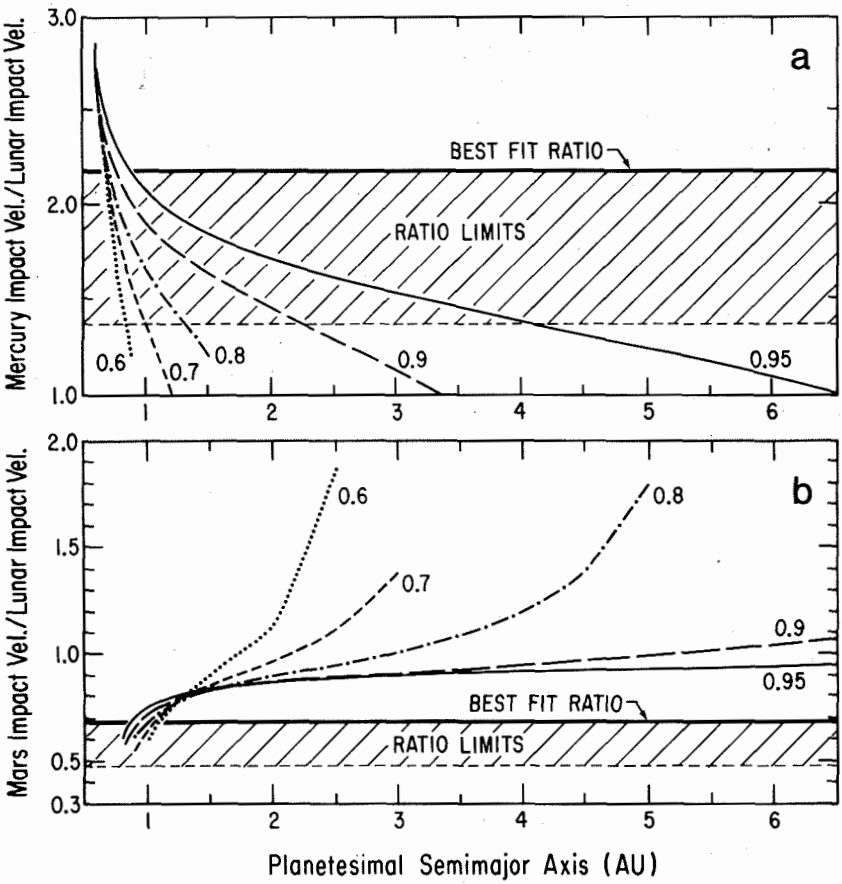

Fig. 19. Plot of the impact velocity ratios Mercury/Moon (a) and Mars/Moon (b) derived from matching the highlands crater curves (Fig. 18), vs impactor semimajor axes for eccentricities from 0.6 to 0.95. The hachured areas are the limiting impact velocity ratios for an acceptable curve fit, while the solid horizontal lines are the ratios derived from the best curve fit shown in Fig. 18. Only planetesimals with semimajor axes between about 0.8 and 1.2 AU lie within the same region of the impact velocity ratio limits. Jupiter crossers have semimajor axes >2.7 AU.

0.5 to 6.5 AU for eccentricities from 0.6 to 0.95. Also shown are the limiting impact-velocity ratios for an acceptable curve fit (hachured areas) and the ratios derived from the best curve fit shown in Fig. 18 (solid horizontal line). Only those parts of the eccentricity curves that lie within the hachured areas have impact-velocity ratios compatible with the observed shifts in the crater size-frequency distributions. The planetesimal orbits are further constrained by the need to have the curves lie within the same parts of the Mercury/Moon and Mars/Moon ratio limits. This occurs only for planetesimals with semimajor axes between about 0.8 and 1.2 AU. No matter what the eccentricity, planetesimals with semimajor axes greater than about 1.2 AU produce Mars/Moon impact velocity ratios that are too high to account for the shift between the Martian and lunar crater curves. The best fit of the crater curves is given by objects with semimajor axes of about 0.85 AU and eccentricities of about 0.95.

These results, together with those shown in Table III for the Moon and Callisto, strongly indicate that the objects responsible for the period of late heavy bombardment on the terrestrial planets were in orbits confined to the inner solar system. These objects are most likely accretional remnants left over from the accretion of the terrestrial planets. Wetherill (1977) has shown that accretional remnants could develop a long-lived tail consistent with the end of late heavy bombardment some 3.8 Gyr ago. This long-lived tail of accretional remnants could have had their orbits pumped up to large eccentricities by close approaches to the inner planets, which is consistent with the large eccentricities giving the best-fit impact-velocity ratios.

If the objects responsible for the period of late heavy bombardment of the terrestrial planets were confined to the inner solar system, then it follows that the period of late heavy bombardment of the outer planet satellites was the result of objects confined to that region of the solar system. Based on cumulative crater frequencies among the Saturnian satellites, Horedt and Neukum (1984) find that the objects responsible for the cratering record were more likely to have been in planetocentric orbits than in heliocentric orbits. Strom (1987*a*) reached a similar conclusion from differences of the crater populations among the outer planet satellites. Therefore, it is possible that the period of late heavy bombardment in the outer solar system was primarily the result of objects in planetocentric orbits. This conclusion should remain tentative until more detailed studies of the cratering record and celestial mechanical studies of planetocentric objects are concluded.

VI. SUMMARY

The cratering records in the lunar, Mercurian and Martian highlands all show similar size-frequency distributions which are characterized by highly structured curves with multiple distribution functions. On Mercury and Mars, there is a significant paucity of craters less than about 40 or 50 km diameter

compared to the Moon. This paucity of craters is probably due to the obliteration of a fraction of craters by intercrater plains emplacement on Mercury and a combination of intercrater plains emplacement and atmospheric erosion and deposition on Mars. Intercrater plains are the major terrain type on Mercury, and both the cratering record and stratigraphic studies strongly indicate that they were emplaced over a period of time during the period of late heavy bombardment. Estimated absolute ages from crater densities suggest intercrater plains range from about 4.0 to 4.2 Gyr which coincides with the period of late heavy bombardment on the Moon. If intercrater plains are volcanic, then Mercury experienced much more volcanic activity during the period of late heavy bombardment than the Moon. This, however, is consistent with thermal history models that predict extensive lithospheric melting, global expansion and crustal extension resulting from the formation of Mercury's enormous iron core. Such conditions would provide a ready source of magma and an ideal tectonic setting for easy egress of lavas to the surface.

The Mercurian smooth plains within and surrounding the Caloris basin have a post-plains crater population that has a size-frequency distribution very similar to that of the lunar highlands over the same diameter range. The crater density is about an order of magnitude less than the Mercurian and lunar highlands, indicating that they are relatively young. The post-Caloris plains crater population, however, has a crater density identical to that superposed on the lunar Orientale basin and ejecta blanket which is about 5 times greater than that superposed on the lunar maria. This suggests that the Mercurian smooth plains were emplaced near the end of late heavy bombardment. They may be, on average, about 3.8 Gyr old, and therefore older than most of the lunar maria. Volcanism may have been shorter lived on Mercury than the Moon because the cooling of the lithosphere and the large iron core could have produced global compression that closed off magma conduits and inhibited volcanism earlier on Mercury than on the Moon. Mercury's cratering record and estimated ages from crater densities suggest that internal activity on Mercury was more extensive early in its history than on the Moon, but that it ended sooner.

The similarity of the crater size-frequency distributions for the heavily cratered surfaces in the inner solar system strongly suggests that they resulted from a single family of impacting objects in heliocentric orbits. The heavily cratered surfaces at Jupiter (Callisto and Ganymede) show a different crater population characterized by a paucity of large craters > 40 km diameter and an overabundance of small craters < 20 km diameter relative to that in the inner solar system. This difference cannot be explained by differences in crater scaling between Jupiter and the inner solar system. The impact velocities required to make the inner solar system and Callisto crater curves coincide are completely incompatible with impact velocities for objects in heliocentric orbits that cross Jupiter and the inner planets. This suggests that the objects responsible for the period of late heavy bombardment on the inner planets were confined to the inner solar system.

The inner planet highlands crater curves are laterally displaced with respect to each other in such a manner that higher impact velocities are required at planets with smaller heliocentric distances. The impact-velocity ratios Mercury/Moon and Mars/Moon derived from the Holsapple-Schmidt crater scaling law, and required to account for the lateral shifts, have fairly narrow ranges. Only objects with semimajor axes between about 0.8 and 1.2 AU are capable of producing the impact velocity ratios derived from the cratering record. The best curve fits require semimajor axes of about 0.85 AU and eccentricities of about 0.95. This strongly indicates that the objects responsible for the period of late heavy bombardment on the inner planets were confined to the inner solar system. These objects were probably accretional remnants left over from the formation of the inner planets. This implies that the outer solar system cratering record was the result of objects confined to that region, possibly in orbits that were mostly planetocentric.